Analysis of Nonsolvent–Solvent–Polymer Phase Diagrams and Their Relevance to Membrane Formation Modeling

L. YILMAZ and A. J. McHUGH, *Department of Chemical Engineering, University of Illinois, Urbana, Illinois 61801*

Synopsis

Calculations have been carried out, based on Flory–Huggins solution theory, to analyze the behavior of the ternary nonsolvent–solvent–polymer phase diagram for typical membrane-forming systems. Consideration is given to the behavior of the spinodal as well as binodal curves, tie-line slopes, and critical points as a function of various parameters, most especially those related to the concentration dependency of the interaction parameters. Implications regarding membrane structure formation are discussed, and the suitability of different functional forms for the interaction parameter concentration dependence is also analyzed.

The net result of these calculations is to demonstrate the importance of the various parameters in controlling the phase-diagram behavior and particularly to show the critical role of the concentration dependence of the solvent–polymer interaction parameter in affecting the nature of the miscibility gap.

INTRODUCTION

Since the invention of the asymmetric membrane by Loeb and Sourirajan,[1] membrane separation processes have attracted considerable commercial interest. Asymmetric membranes are generally prepared by phase inversion techniques,[2] the principal steps of which involve casting of a thin film of homogeneous polymer solution onto a suitable substrate, followed by quenching in a nonsolvent bath to precipitate the membrane film. In some cases, the nonsolvent quench is preceded by a short evaporation period; however, this step is not necessary to obtain an asymmetric structure.[3] The precipitated film may also be heat treated to densify the structure.

The principal structure-forming processes occur during the quenching step during which solvent–nonsolvent exchange occurs accompanied by various phase transformations. It seems clear, therefore, that mathematical models for this process should address both the thermodynamic and kinetic aspects of the system. The thermodynamics involves construction of the complete ternary phase diagram for the nonsolvent–solvent–polymer system (NS-S-P) and evaluation of the effects of the phase diagram characteristics on the formation of a given membrane structure. The kinetic aspect of the modeling involves the construction of a proper diffusion equation formalism for the mass transfer which would enable calculation of fluxes and concentration profiles during the precipitation processes.[4] In this paper, we shall be concerned with an assessment of the thermodynamics of the ternary NS-S-P system.

Early studies of ternary NS-S-P systems were limited largely by the re-

Journal of Applied Polymer Science, Vol. 31, 997–1018 (1986)
 CCC 0021-8995/86/040997-22$04.00

strictive assumptions needed to reduce the complexity of the phase diagram calculations. For example, Scott[5] employed restraints on the interaction parameters, such as treating the NS-S as a single fluid or assuming complete incompatibility of the nonsolvent and polymer. In other cases, assumptions were made regarding equality of the NS-S and S-P interaction parameters and neglect of the NS-P interaction parameter, or infinite molecular weight was assumed. Krigbaum and Carpenter,[6] and later Suh and Liou,[7] assumed that the polymer concentration in the dilute liquid phase could be neglected, which can be reasonable for some cases; however, they calculated specific combinations of compositions such as $R = (\phi_{1,A}/\phi_{2,A}) / (\phi_{1,B}/\phi_{2,B})$, (where the ϕ's are volume fractions and the subscripts refer to the nonsolvent (1), solvent (2), and concentrated phase A or dilute phase B rather than to the entire phase diagram. Further, more detailed summaries of the earlier work can be found in Tompa.[8]

A more complete series of calculations of membrane-forming systems has recently been published by Altena and Smolders,[9] in which comparisons were made of binodal curves calcualted using Flory–Huggins theory and experimental cloud-point measurements. Their calculations dealt mainly with binodal curves and assumed a concentration dependency only for the nonsolvent–solvent pair, treating the other two as constants. Because their primary concern was with comparisons to miscibility gap data, analysis of the characteristics of the phase diagrams for a wide range of parameter sets was not attempted. In a number of membrane formation models,[4,10,11] the region of complete instability, i.e., spinodal, plays an important role. In addition, a large number of experimental studies have shown that solvent–polymer binary interaction parameters can in fact exhibit strong concentration dependencies.[12–16] Such behavior we feel can have an important bearing on the understanding of both the phase separation and structure formation processes in membrane formation. Our aim therefore has been to consider rigorously all aspects of NS-S-P phase diagram behavior (i.e., the spinodal as well as binodal curves, tie-line slopes, and critical points) and the effects of variations of the interaction parameters on the phase diagram characteristics as well as their relevance of membrane formation. The suitability of different functional forms for the concentration dependency has also been considered. In our calculations the polymer is assumed to be monodisperse.

DEVELOPMENT OF EQUATIONS

Our description of the thermodynamics of the NS-S-P system is based on the well-established Flory–Huggins theory.[8,17] Although the more recently developed corresponding states or equation-of-state methods are, in principal, more rigorous, their utility is severely restricted by the increased complexity of the calculations and limited data base.[18,19] Their use has also generally been limited to the description of binary systems with rare extension to the ternary case.[20] In order to obtain better agreement with experimental data, Flory–Huggins theory can be empirically extended through use of concentration-dependent interaction parameters g_{ij}. This

has been the preferred form in our calculations. Thus, for the Gibbs free energy of mixing one has:[21,22]

$$\frac{\Delta G_M}{RT} = n_1 \ln\phi_1 + n_2 \ln\phi_2 + n_3 \ln\phi_3 + g_{12}(u_2) n_1 \phi_2 + g_{13}(\phi_3) n_1 \phi_3 + g_{23}(\phi_3) n_2 \phi_3 \tag{1}$$

In eq. (1), n_i are moles, and the quantities u_1 and u_2 are given by $u_2 = \phi_2/(\phi_1 + \phi_2)$ and $u_1 = \phi_1/(\phi_1 + \phi_2)$. The subscripts refer to nonsolvent (1), solvent (2), and polymer (3). The suggested ternary correction term[18,21] has been omitted because its inclusion introduces an excessive number of parameters and there are no data available to evaluate the correction term for membrane-forming systems. Use of the definition for the chemical potential: $\frac{\Delta\mu_i}{\mathrm{RT}} = \frac{\partial}{\partial n_i}\left(\frac{\partial \Delta G_M}{RT}\right)_{n_j, j \neq i}$ leads to the following expressions:

$$\frac{\Delta\mu_1}{RT} = \ln\phi_1 + 1 - \phi_1 - \frac{\nu_1}{\nu_2}\phi_2 - \frac{\nu_1}{\nu_3}\phi_3 + (g_{12}\phi_2 + g_{13}\phi_3)(\phi_2 + \phi_3) - g_{23}\frac{\nu_1}{\nu_2}\phi_2\phi_3 - u_1 u_2 \phi_2 \left(\frac{dg_{12}}{du_2}\right) - \phi_1\phi_3{}^2\left(\frac{dg_{13}}{d\phi_3}\right) - \frac{\nu_1}{\nu_2}\phi_2\phi_3{}^2\left(\frac{dg_{23}}{d\phi_3}\right) \tag{2}$$

$$\frac{\Delta\mu_2}{RT} = \ln\phi_2 + 1 - \phi_2 - \frac{\nu_2}{\nu_1}\phi_1 - \frac{\nu_2}{\nu_3}\phi_3 + \left(g_{12}\frac{\nu_2}{\nu_1}\phi_1 + g_{23}\phi_3\right)(\phi_1 + \phi_3) - g_{13}\frac{\nu_2}{\nu_1}\phi_1\phi_3 + u_1 u_2 \frac{\nu_2}{\nu_1}\phi_1\left(\frac{dg_{12}}{du_2}\right) - \frac{\nu_2}{\nu_1}\phi_1\phi_3{}^2\left(\frac{dg_{13}}{d\phi_3}\right) - \phi_2\phi_3{}^2\left(\frac{dg_{23}}{d\phi_3}\right) \tag{3}$$

$$\frac{\Delta\mu_3}{RT} = \ln\phi_3 + 1 - \phi_3 - \frac{\nu_3}{\nu_1}\phi_1 - \frac{\nu_3}{\nu_2}\phi_2 + \left(g_{13}\frac{\nu_3}{\nu_1}\phi_1 + g_{23}\frac{\nu_3}{\nu_2}\phi_2\right)(\phi_1 + \phi_2) - g_{12}\frac{\nu_3}{\nu_1}\phi_1\phi_2 + \left[\frac{\nu_3}{\nu_1}\phi_1\left(\frac{dg_{13}}{d\phi_3}\right) + \frac{\nu_3}{\nu_2}\phi_2\left(\frac{dg_{23}}{d\phi_3}\right)\right]\phi_3(\phi_1 + \phi_2) \tag{4}$$

In eqs. (2) to (4), ν_i represents the pure molar volume of species i. Solution for the binodal curve requires:

$$\Delta\mu_{i,A} = \Delta\mu_{i,B} \quad i = 1,2,3 \tag{5}$$

subject to the material balance constraints, $\Sigma\phi_{i,A} = \Sigma\phi_{i,B} = 1$. Subscripts A and B refer to the polymer-rich and dilute phases, respectively.

Selection of one of the compositions as an independent variable leaves five coupled nonlinear algebraic equations to be solved for the individual tie lines.

Analysis of the limit of the unstable region is also of importance in understanding the phase separation behavior of membrane-forming systems. Thus the spinodal can be evaluated from the relation for ternary systems:[8]

$$G_{23}\,G_{33} = (G_{23})^2 \tag{6}$$

where $G_{ij} = \left(\frac{\partial^2 \overline{\Delta G}_M}{\partial\phi_i\,\partial\phi_j}\right)\nu_{\text{ref}}$, and ν_{ref} is the molar volume of the reference component, which in our case we take to be component 1.

From the relationship for $\overline{\Delta G}_M$ (on a unit-volume basis), one has:

$$\left(\frac{\partial\overline{\Delta G}_M}{\partial\phi_2}\right)_{T,P,\phi_3} = \frac{\Delta\mu_2}{\nu_2} - \frac{\Delta\mu_1}{\nu_1} \tag{7}$$

$$\left(\frac{\partial\overline{\Delta G}_M}{\partial\phi_3}\right)_{T,P,\phi_2} = \frac{\Delta\mu_3}{\nu_3} - \frac{\Delta\mu_1}{\nu_1} \tag{8}$$

Thus from eqs. (2) to (4), the following expressions result:

$$\begin{aligned}\left(\frac{\partial\overline{\Delta G}_M/RT}{\partial\phi_2}\right)_{T,P,\phi_3} &= \frac{1}{\nu_2}\ln\phi_2 - \frac{1}{\nu_1}\ln\phi_1 + \frac{1}{\nu_2} - \frac{1}{\nu_1} \\ &+ \left(g_{12}\frac{\phi_1}{\nu_1} + g_{23}\frac{\phi_3}{\nu_2}\right)(1-\phi_2) - g_{13}\frac{\phi_1\phi_3}{\nu_1} \\ &- \left(g_{12}\frac{\phi_2}{\nu_1} + g_{13}\frac{\phi_3}{\nu_1}\right)(\phi_2 + \phi_3) + g_{23}\frac{\phi_2\phi_3}{\nu_2} \\ &+ \frac{\phi_1{}^2\phi_2}{\nu_1(1-\phi_3)^2}\left(\frac{dg_{12}}{du_2}\right) + \frac{\phi_1\,\phi_2{}^2}{\nu_1(1-\phi_3)^2}\left(\frac{dg_{12}}{du_2}\right)\end{aligned} \tag{9}$$

$$\begin{aligned}\left(\frac{\partial\overline{\Delta G}_M/RT}{\partial\phi_3}\right)_{T,P,\phi_2} &= \frac{1}{\nu_3}\ln\phi_3 + \frac{1}{\nu_3} - \frac{1}{\nu_1}\ln\phi_1 - \frac{1}{\nu_1} \\ &+ \left(g_{13}\frac{\phi_1}{\nu_1} + g_{23}\frac{\phi_2}{\nu_2}\right)(1-\phi_3) - g_{12}\frac{\phi_1\phi_2}{\nu_1} \\ &+ \frac{\phi_1\phi_3}{\nu_1}\frac{dg_{13}}{d\phi_3} + \frac{\phi_2\phi_3}{\nu_2}\left(\frac{dg_{23}}{d\phi_3}\right) - \left(g_{12}\frac{\phi_2}{\nu_1} + g_{13}\frac{\phi_3}{\nu_1}\right)(\phi_2 + \phi_3) \\ &+ g_{23}\frac{\phi_2\phi_3}{\nu_2} + \frac{\phi_1\phi_2{}^2}{\nu_1(1-\phi_3)^2}\left(\frac{dg_{12}}{du_2}\right)\end{aligned} \tag{10}$$

From the last two equations one can derive the necessary expressions for the spinodal.*

$$G_{22} = \frac{1}{\phi_1} + \frac{\nu_1}{\nu_2\phi_2} - 2g_{12} + 2(u_1 - u_2)\left(\frac{dg_{12}}{du_2}\right) + u_1u_2\left(\frac{d^2g_{12}}{du_2{}^2}\right) \tag{11}$$

$$G_{23} = \frac{1}{\phi_1} - (g_{12} + g_{13}) + \frac{\nu_1}{\nu_2} g_{23} + u_2\,(u_1 - 2u_2)\left(\frac{dg_{12}}{du_2}\right) + u_1u_2{}^2\left(\frac{d^2g_{12}}{du_2{}^2}\right) - \phi_3\left(\frac{dg_{13}}{d\phi_3}\right) + \frac{\nu_1}{\nu_2}\phi_3\left(\frac{dg_{23}}{d\phi_3}\right) \tag{12}$$

$$G_{33} = \frac{1}{\phi_1} + \frac{\nu_1}{\nu_3\phi_3} - 2g_{13} - 2u_2{}^2\,(1-u_1)\left(\frac{dg_{12}}{du_2}\right) + u_1u_2{}^3\left(\frac{d^2g_{12}}{du_2{}^2}\right) + 2\,(\phi_1-\phi_3)\left(\frac{dg_{13}}{d\phi_3}\right) + \phi_1\phi_3\left(\frac{d^2g_{13}}{d\phi_3{}^2}\right) + \frac{2\nu_1}{\nu_2}\phi_2\left(\frac{dg_{23}}{d\phi_3}\right) + \frac{\nu_1}{\nu_2}\phi_2\phi_3\left(\frac{d^2g_{23}}{d\phi_3{}^2}\right) \tag{13}$$

To calculate the spinodal curve, one of the compositions is chosen as the independent variable which, in conjunction with the material balance, $\Sigma\,\phi_i = 1$, results in a single nonlinear equation to be solved.

The critical point for a ternary system is given by:[8]

$$G_{222}G_{33}{}^2 - 3\,G_{223}G_{23}G_{33} + 3G_{233}G_{23}^2 - G_{22}G_{23}G_{333} = 0 \tag{14}$$

For the special case of constant g_{ij}, eq. (14) reduces to:

$$1 - \frac{\nu_1}{\nu_2}\left(\frac{\phi_1{}^c}{\phi_2{}^c}\right)^2 - 2\,\frac{G_{22}}{G_{23}}\left(1 - \frac{G_{22}}{G_{23}}\right) - 1 - \frac{\nu_1}{\nu_3}\left(\frac{\phi_1{}^c}{\phi_3{}^c}\right)^2\left(\frac{G_{22}}{G_{23}}\right)^3 = 0 \tag{15}$$

METHOD OF COMPUTATION

Reported methods for calculating phase diagrams in ternary systems have generally been based on a least-squares procedure for minimizing a suitably chosen objective function.[9,23,24] In our case we have used ΣF_i^2 as our objective function, where

$$F_i = (\Delta\mu_{i,A} - \Delta\mu_{i,B})/RT \quad i = 1,2,3 \tag{16a}$$

* For constant g_{13} and g_{23}, these equations should simplify to the expressions given by eqs. (8) to (10) of Ref. (9). Although this is true for the G_{22} expression, our expressions yield terms in $\frac{dg_{12}}{du_2}$ and $\frac{d^2g_{12}}{du_2{}^2}$ for G_{23} and G_{33} which differ from those of (9). The source of this discrepancy is not known.

$$F_4 = 1 - \Sigma \phi_{i,A} \tag{16b}$$

$$F_5 = 1 - \Sigma \phi_{i,B} \tag{16c}$$

Subroutine ZSCNT from the IMSL library was employed, which uses only chemical potential expressions for input. A serious complication in the numerical calculation of the binodal is the existence of a trivial solution, where $\phi_{i,A} = \phi_{i,B}$. As a means for overcoming this problem, Hsu and Prausnitz[23] employed a penalty function in the form:

$$F_i = \frac{(\Delta\mu_{i,A} - \Delta\mu_{i,B})/RT}{(\phi_{i,A} - \phi_{i,B})^r}$$

with $r = 1$ or 2. In our computations we have found that the introduction of penalty functions leads to little improvement in avoiding trivial solutions, and in many cases creates local extrema which trap the iterative procedure. Altena and Smolders[9] have indicated that the use of a subroutine from the NAG library, requiring expressions for the first and second derivatives of the chemical potentials, avoids trivial solutions without the need of penalty functions. Likewise, difficulties arise in the calculations when one of the ϕ_i values becomes very small, causing the search routine to assume negative values and thus stoppage due to negative logarithmic arguments.

To deal with these problems we have used the fact that for large portions of the binodals, polymer compositions in the dilute phase are near zero (Altena and Smolders,[9] for example, have noted that $\phi_{3,B}$ can be as small as 10^{-30}, whereas in our calculations values as low as 10^{-90} result, which are of course physically meaningless). Also, in general, values of $\phi_{3,B}$ are found to be closest to zero, relative to the other compositions for given tie lines, throughout the entire phase diagram. We therefore have selected $\phi_{3,B}$ as our independent variable because choice of any of the other five compositions often leads to nonconvergence. We have also found added flexibility in working with the full five-unknown, five-equation system rather than the 3×3 system obtained from substitution of the material balance expressions. In order to avoid trivial solutions, initial guesses for the phase compositions must be close to the correct values, which is difficult to achieve for all tie lines. We therefore use results of a previous tie-line calculation (i.e., values of $\phi_{i,A}$, $i = 1,2,3$ and $\phi_{i,B}$, $i = 1,2$) as the initial guess for the succeeding calculation. Provided that distances between successive tie lines are not too large, such a scheme works well, and, if the initial guess for the first tie line is sufficiently accurate, the entire binodal curve can be generated without recourse to further guessing. In our algorithm, calculations are started close to the polymer–nonsolvent line and proceed through the critical point, because in this region the miscibility gap is largest, thus more easily avoiding trivial solutions.

Because for large portions of the dilute branch of the binodal curve, extremely small and physically meaningless polymer concentrations result, the calculation procedure can be simplified by assuming that the dilute phase contains zero polymer until the neighborhood of the critical point. Thus expressions for the chemical potential simplify to the following:

$$\frac{\Delta\mu_{1,B}}{RT} = \ln\phi_{1,B} + (1 - \frac{\nu_1}{\nu_2})\,\phi_{2,B} + g_{12}\,\phi_{2,B}^2 - \phi_{1,B}\,\phi_{2,B}^2\left(\frac{dg_{12}}{d\phi_{2,B}}\right) \quad (17a)$$

and

$$\frac{\Delta\mu_{2,B}}{RT} = \ln\phi_{2,B} + (1 - \frac{\nu_2}{\nu_1})\phi_{1,B} + \frac{\nu_2}{\nu_1}g_{12}\phi_{1,B}^2 + \frac{\nu_2}{\nu_1}\,\phi_{2,B}\phi_{1}B^2\left(\frac{dg_{12}}{d\phi_{2,B}}\right) \quad (17b)$$

where now $g_{12} = g_{12}(\phi_{2,B})$.

For $\Delta\mu_{1,B}$ and $\Delta\mu_{2,A}$, eqs. (2) and (3) are used. Because this portion of the dilute branch of the binodal curve will fall on the solvent–nonsolvent line, $\phi_{2,B}$ is chosen as the independent variable, and $\phi_{1,B}$ is calculated from $\phi_{1,B} + \phi_{2,B} = 1.0$. Solving for the remaining three unknowns $\phi_{i,A}$ $(i = 1,2,3)$ then requires use of:

$$\Delta\mu_{i,A} = \Delta\mu_{i,B} \quad i = 1,2 \quad (18a)$$

and

$$\Sigma\phi_{i,A} = 1 \quad (18b)$$

Up to values of $\phi_{3,B}$ on the order of 10^{-4}, the accuracy (to within five digits) of the results is equal to that realized from solution of the original system of equations. In addition, calculations are less sensitive to the initial guess and on the order of two to three times faster. The algorithm starts from the solvent-poor side, using eqs. (17) and (18) to calculate tie lines, until the region of the critical point where the switch is made to the full system of equations, using the last calculated tie line as the initial guess from which to proceed.

In the case of the spinodal curve, the same numerical procedure was employed with ϕ_3 as the independent variable, eliminating the other through the material balance. This leaves a single nonlinear equation to be solved. As in the case of the binodal curve, previous point values were used as first guesses for calculating successive values. Finally, calculation of critical points followed the same procedure employed to solve the simultaneous equations described above.

RESULTS AND DISCUSSION

Constant Interaction Parameter

For the case of constant interaction parameters, there are five quantities whose values need fixing (g_{12}, g_{13}, g_{23}, ν_1/ν_2, ν_1/ν_3). In order to examine the phase diagram characteristics that are relevant to membrane formation processes, we have chosen arbitrary sets of values of these parameters consistent with typical NS-S-P systems to generate binodal and spinodal curves. In addition to the position and shape of the miscibility gap (binodal

curve), the relative position and shape of the spinodal gap is of importance in modeling membrane formation.[4,10,11] Slopes of the tie lines are also considered to be of some importance in the determination of overall porosities of membrane layers.

Figure 1 shows two sets of binodal and spinodal curves and illustrates several general features characteristic of membrane-forming systems. The two sets of parameters used in this case are those for the water–acetone–cellulose acetate system as given by Altena and Smolders[9] ($g_{12} = 0.5$) and Cohen et al.[10] ($g_{12} = -0.3$). An important feature in both cases is the considerable change in the slopes of the tie lines that occurs over the two-phase region, with changes increasing as the miscibility gap increases. Similar behavior was seen for a range of parameter sets. Such behavior indicates that during the nonsolvent quench, the point of entry into the region of immiscibility as well as the total system composition (i.e., position on the ternary diagram) at which phase separation begins will have a strong bearing on the porosity of the precipitated layers. Calculation of the sequential buildup of porosity would require a knowledge of both the location and slope of the tie lines. In addition to the large quantitative difference in the two phase diagrams of Figure 1, an important qualitative feature shows up in the behavior predicted on the basis of the parameters from Ref. 10. Both the binodal and spinodal curves for this case exhibit a maximum in polymer concentration, and the same tie line passes through both points. Thus, for a polymer concentration above the maximum binodal point for this system, no amount of nonsolvent would lead to phase separation or entrance to the unstable region.

For concentrations beneath the binodal maximum but above the spinodal maximum, entrance to the unstable region by further addition of nonsolvent would not be possible. Examination of Figures 3–5 in the Cohen et al. paper clearly shows that such maxima play a role in their predictions of porous membrane formation.

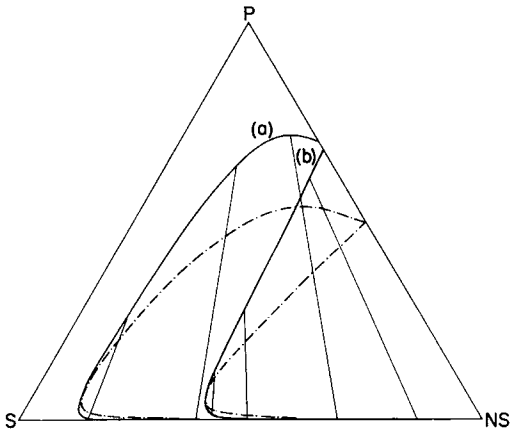

Fig. 1. Phase diagrams with several representative tie lines for water–acetone–cellulose acetate system. Binodal (–) and spinodal (–•–) curves: (a) $g_{12} = -0.3$, (b) $g_{12} = 0.5$. Other parameters are $\nu_1/\nu_2 = 0.25$, $\nu_1/\nu_3 = 0.002$, $g_{13} = 1.0$, and $g_{23} = 0.2$.

A behavior pattern similar to that illustrated by Figure 1 occurred for a wide range of interaction parameter values, several of which are illustrated in Figures 2–4. In each case the binodal and spinodal maxima, when they occurred, did so together, and a common tie line passed through each. The relative flatness of the spinodal maximum implies the existence of a large metastable region in the neighborhood of $\phi_{3,max.}$ Changes in the magnitudes of the interaction parameters shift the miscibility gap and therefore maxima locations; however, their existence is largely controlled by the value of g_{12}. These figures illustrate that the sharpness of the maxima clearly increases with decreasing g_{12}, becoming most pronounced for negative values (maxima were never observed for $g_{12} > 0.05$). Also, to some extent, increased g_{23} values lead to a small increase in the value of g_{12}, needed for the existence of a maximum. One therefore concludes that a high affinity between the nonsolvent and solvent (low g_{12}) can have important qualitative as well as quantitative consequences on the phase diagram. Such a result is in agreement with observations made in the literature regarding the importance of solvent–nonsolvent affinity in membrane formation.

Another important pattern relates to the nonsolvent concentration necessary to cause precipitation for a given polymer concentration and its relation to membrane properties, a feature that has been studied experimentally.[25,26] The behavior of $\phi_{1,A}$ with changes in $\phi_{3,A}$ varies widely for different parameter sets as illustrated by Figures 3 and 4. For largely immiscible systems, the volume fraction of nonsolvent in the polymer-rich phase remains essentially constant over the major portion of the miscibility gap. In general, one would expect that for the main portion of the binodal curve, nonsolvent concentration at the cloud point would decrease with increasing polymer concentration. However, the opposite pattern more often occurs and is especially pronounced in cases where the polymer maximum behavior is seen. On the other hand, systems showing a decrease in nonsolvent concentration with increasing polymer, though rare, do occur in cases where the miscibility is high as a consequence of large solvent–nonsolvent interactions (g_{12}), as shown in Figures 1 and 4.

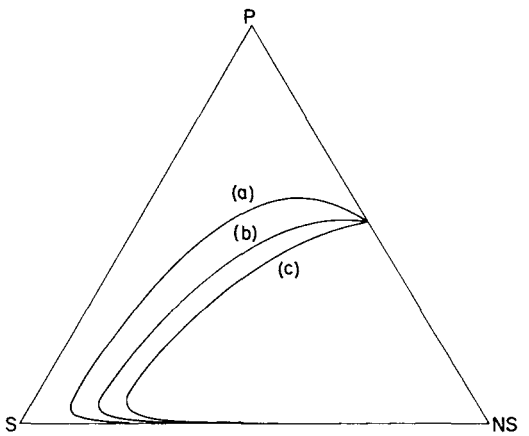

Fig. 2. Spinodal curves for various g_{12}: (a) $g_{12} = -0.5$, (b) $g_{12} = -0.1$ (c) $g_{12} = 0.1$. Other parameters are $\nu_1/\nu_2 = 0.25$, $\nu_1/\nu_3 = 0.002$, $g_{13} = 1.0$, and $g_{23} = 0.2$.

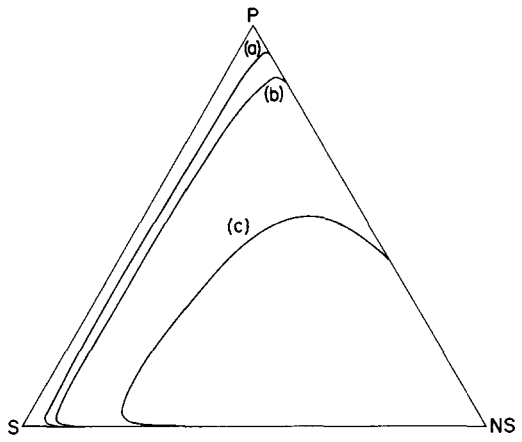

Fig. 3. Binodal curves for various g_{13}: (a) $g_{13} = 2.0$, (b) $g_{13} = 1.5$, (c) $g_{13} = 0.7$. Other parameters are $\nu_1/\nu_2 = 0.25$, $\nu_1/\nu_3 = 0.002$, $g_{12} = -0.3$, and $g_{23} = 0.2$.

The effect of polymer molecular weight on the phase diagram can be analyzed through variations of the quantity ν_1/ν_3 and is illustrated in Figure 5 for the binodal, which is typical of that observed over a wide range of g_{ij} values. One sees that the polymer-rich branch is relatively insensitive to molecular weight until the polymer concentration drops below $\sim$ 15%, after which the expected trend of increased miscibility with decreased molecular weight occurs. At the same time, changes in the slopes of the tie line become significant in this region. Trends in the spinodal are roughly similar, except that the effects are somewhat larger. The effect of molecular weight on the critical point and, in particular, on the value of polymer volume fraction at the critical point, ϕ_3^c, is important in controlling which phase precipitates (either the polymer-rich or the polymer-poor), thereby forming the discontinous phase.[27] Results for the polymer critical point are shown in Table I and illustrate that critical concentrations can drop dra-

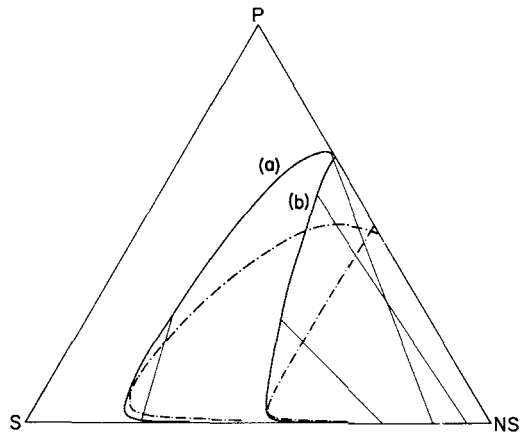

Fig. 4. Phase diagrams showing binodal (–) and spinodal (–•–) curves and several tie lines for two sets of g_{ij} values: (a) $g_{12} = 1.0$, $g_{13} = 1.0$, $g_{23} = 0.5$; (b) $g_{12} = 0.0$, $g_{13} = 1.0$, $g_{23} = 0.0$. Other parameters are $\nu_1/\nu_2 = 0.2$, $\nu_1/\nu_3 = 0.002$.

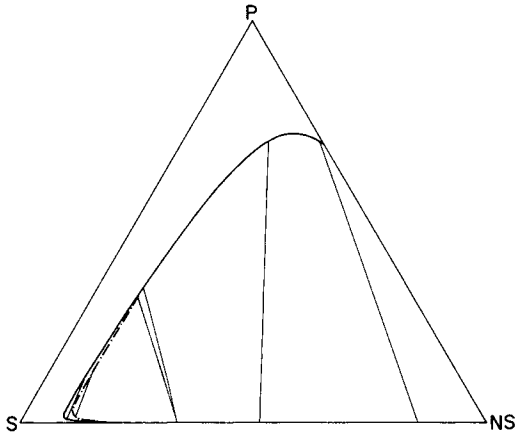

Fig. 5. Binodal curves for two different molecular weights: (–) $\nu_1/\nu_3 = 0.0001$; (–·–) $\nu_1/\nu_3 = 0.001$. Other parameters are $g_{12} = 0.3$, $g_{13} = 1.0$, and $g_{23} = 0.2$.

matically with increases in polymer molecular weight, whereas the effect on the solvent and nonsolvent concentrations is less pronounced. Table II illustrates the less pronounced effects of the interaction parameters on the critical concentrations. One concludes, therefore, that molecular weight is indeed the controlling factor for ϕ_3^c.

Concentration Dependent Interaction Parameters

As pointed out earlier, the principal reason for employing concentration-dependent forms for the interaction parameters has been to improve the accuracy of the phase diagrams predicted from Flory–Huggins theory. In our case, we have been concerned with the question of whether inclusion of concentration-dependent forms produces significant changes in the phase diagram and, if so, what effects this has on the qualitative features as well,

TABLE I
Effect of Molecular Weight on Critical Point Compositions

A. $g_{12} = -0.3$, $g_{13} = 1.0$, $g_{23} = 0.2$, $\nu_1/\nu_2 = 0.25$

ν_1/ν_3	ϕ_1^c	ϕ_2^c	ϕ_3^c
0.01	0.144	0.730	0.126
0.002	0.106	0.832	0.062
0.001	0.098	0.852	0.045
0.0001	0.085	0.900	0.015

B. $g_{12} = 0.5$, $g_{13} = 1.0$, $g_{23} = 0.2$, $\nu_1/\nu_2 = 0.25$

ν_1/ν_3	ϕ_1^c	ϕ_2^c	ϕ_3^c
0.01	0.439	0.459	0.102
0.002	0.375	0.570	0.054
0.001	0.359	0.601	0.040
0.0001	0.332	0.654	0.014

TABLE II
Effect of Interaction Parameters on Critical Point Compositions

$\nu_1/\nu_2 = 0.25$, $\nu_1/\nu_3 = 0.002$

A. $g_{13} = 1.5$, $g_{23} = 0.2$

g_{12}	ϕ_1^c	ϕ_2^c	ϕ_3^c
-0.5	0.046	0.899	0.055
-0.2	0.061	0.882	0.057
0.1	0.084	0.857	0.059
0.4	0.122	0.819	0.059
0.7	0.182	0.761	0.057
1.0	0.263	0.690	0.047

B. $g_{12} = 0.5$, $g_{23} = 0.2$

g_{13}	ϕ_1^c	ϕ_2^c	ϕ_3^c
0.7	0.717	0.241	0.042
1.0	0.375	0.571	0.054
1.3	0.199	0.742	0.059
1.6	0.119	0.823	0.058
1.9	0.079	0.865	0.056
2.2	0.056	0.890	0.054
2.5	0.042	0.906	0.052

C. $g_{12} = -0.3$, $g_{13} = 1.0$

g_{23}	ϕ_1^c	ϕ_2^c	ϕ_2^c
-0.5	0.254	0.698	0.048
-0.3	0.217	0.732	0.051
-0.1	0.176	0.770	0.054
0.1	0.130	0.811	0.059
0.3	0.081	0.854	0.065
0.5	0.027	0.898	0.075

such as shapes, slopes of the tie lines, etc. In our analysis of the available data on binary interaction pairs, we have been further motivated to develop an understanding of which empirical forms fit the data best and what typical parameter ranges would be. In such a fashion, one can gain an appreciation of the effect of the concentration dependence on the shape of the binodal and spinodal curves for typical membrane-forming systems.

Because the swelling equilibrium method generally used to obtain interaction-parameter data for nonsolvent–polymer pairs is limited to single values,[28] one obviously cannot generate information on the concentration dependence of g_{13}. We have thus assumed this parameter to be constant and therefore focus our attention in what follows on an examination of the concentration dependencies of g_{12} and g_{23}.

Solvent–Nonsolvent Parameters

Data for low-molecular-weight, binary systems are generally presented in the form of excess Gibbs energy, ΔG^E, versus mole fraction and therefore, for our use, need to be converted to g_{12} versus volume fraction. The latter is easily done through the assumption of constant molar volume inherent in regular soluton theory. To convert ΔG^E to g_{12} on the basis of "strictly regular" solution behavior, one would use the following relationship.[29,30]

$$g_{12} = \frac{\Delta G^E}{RT x_1 x_2} \tag{19}$$

where the x_i represent mole fractions. On the other hand, if one assumes

that Flory–Huggins theory can be applied to solvent–nonsolvent systems, the following expression would result:[31]

$$g_{12} = \frac{1}{x_1\phi_2}\left[x_1 \ln\left(\frac{x_1}{\phi_1}\right) + x_2 \ln\left(\frac{x_2}{\phi_2}\right) + \frac{\Delta G^E}{RT}\right] \tag{20}$$

Because the binary correlations are to be used for ternary-phase diagram calculations, they should be compatible with the limiting binary form obtained from the ternary equations (eqs. 2–4) for $\phi_3 = 0$. Equation (20) exhibits this character. Also in many cases, the actual ΔG^E data have been obtained using correlations, such as the Wilson equation,[32] which are based on nonregular solution theory. For these reasons, eq. (20) was taken as the preferred form for converting data.

Although some authors[9] have used up to five adjustable parameters to fit the g_{12} versus ϕ_2 data, we feel that the limited number of data points, as well as empirically modified theory, does not warrant such a "high-order" fit. Our fits have therefore been limited to first- and second-order polynomials. Strictly for comparison purposes, we have also considered a three-parameter rational form given by:

$$g_{12} = \alpha + \frac{\beta}{1 - \gamma\phi_2} \tag{21}$$

where γ, β, and γ are empirical coefficients. This form was originally suggested by Koningsveld and Kleintjens[33] on semitheoretical grounds for polymer–solvent systems. We have included it here as a proper limiting form for later comparison to our g_{23} calculations. In all cases, coefficients were determined via a modified Marquardt nonlinear regression algorithm.

Table III shows the range of coefficients found for typical system fits and also gives an indication of the suitability of a given correlation form. It is interesting to note that though eq. (21) is strictly applicable to polymer systems, it leads to a better fit than the polynomial form.

Before proceeding to detailed illustrations of the effecets of the various forms in Table III on the ternary-phase diagram, we feel it worthwhile to clear up the discrepancy between our spinodal expressions and those of Altena and Smolders[9] alluded to earlier in our footnote. Although these authors presented equations, no plots or discussion of spinodals has been given. Consequently we present in Figure 6 a comparison of the spinodal curves, using both equation sets together with the common binodal. One clearly sees that our set of equations leads quite properly to a coincidence of the binodal and spinodal curves at the critical point, wheras the spinodal calculated on the basis of the previous authors' equations does not. Such behavior was seen for different g_{12} functions, and we therefore have concluded that an error must exist in their equations.

Figures 7–10 illustrate several characteristics in the behavior of the binodal and spinodal curves resulting from use of the concentration-dependent g_{12}. For the first two cases listed in Table III, the parabolic and rational

TABLE III
Concentration-Dependent Nonsolvent–Solvent Interaction Parameters

System	Range of interaction parameters	Coefficient for $g_{12} = a + b\phi_2 + c\phi_3$			Sum of squares	Coefficients for $g_{12} = \alpha + \beta/(1 - \gamma\phi_2)$			Sum of squares	Reference
		a	b	c		α	β	γ		
H_2O–DMF	0.5–0.9	.504	.057	.348	3.46×10^{-4}	.218	.276	.622	3.08×10^{-5}	22
H_2O–DMSO	(−0.25)–(−0.7)	−.218	−.816	.383	6.31×10^{-3}	−1.302	1.08	−.860	8.49×10^{-3}	23
H_2O–acetone	1.0–2.2	1.141	−.457	1.528	1.78×10^{-2}	0.661	0.417	.755	1.5×10^{-4}	21
H_2O–dioxane	0.92–2.2	.946	−.115	1.383	2.07×10^{-2}	0.340	0.558	.741	6.25×10^{-3}	24

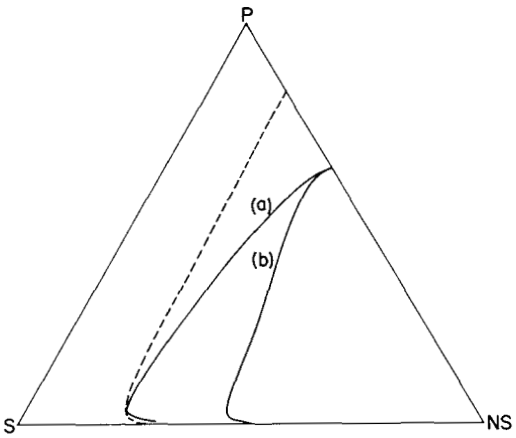

Fig. 6. Spinodal curves calculated (a) from this work, and (b) from the equation given in Ref. (9). Parameters are $\nu_1/\nu_2 = 0.2$, $\nu_1/\nu_3 = 0.002$, $g_{13} = 1.4$, $g_{23} = 0.2$, and $g_{12} = 0.507 + .057u_2 + .348u_2^2$. Binodal curve is shown by dashed line.

forms gave essentially similar results, whereas for H_2O–acetone and H_2O–dioxane systems, slightly different behavior patterns resulted, as shown in Figure 7. In general, shapes of the binodals were less sensitive to the different interaction-parameter correlations than were the tie-line slopes. Changes in the spinodals generally fell between the two. Figure 8 shows a comparison of phase diagrams calculated, respectively, with and without the two concentration-dependent forms, and clearly shows that a reasonably selected constant g_{12} yields a phase diagram very similar to the concentration-dependent case. Similar trends are true for the system illustrated in Figure 9. In this case, polymer maxima are again observed because g_{12} is negative over the range.

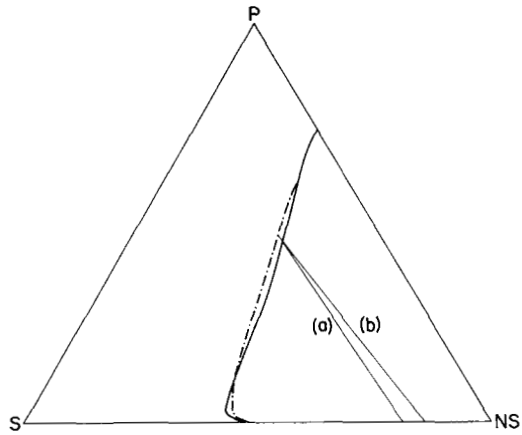

Fig. 7. Binodal curves based on H_2O–acetone data for g_{12}. Solid curve (–) for $g_{12} = 1.141 - 0.47u_2$ and associated tie line (a); broken curve (–•–) for $g_{12} = 0.661 + \dfrac{0.417}{1 - 0.755u_2}$ and associated tie line (b). Other parameters are $\nu_1/\nu_2 = 0.25$, $\nu_1/\nu_3 = 0.002$, $g_{13} = 1.1$, and $g_{23} = 0.4$.

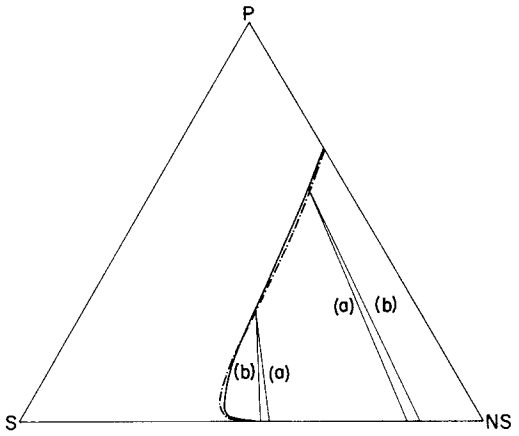

Fig. 8. Binodal curves for (–) concentration-dependent g_{12} ($g_{12} = 0.504 + 0.057u_2 + 0.348u_2^2$) with associated tie lines (a); and for (–•–) constant g_{12} ($g_{12} = 0.6$) with associated tie lines (b). Other parameters are $\nu_1/\nu_2 = 0.2$, $\nu_1/\nu_3 = 0.002$, $g_{13} = 1.0$, and $g_{23} = 0.2$.

For the systems listed in Table III that are characterized by larger g_{12} values and stronger concentration dependencies, the agreement between the binodals calculated with and without constant g_{12} is not as close (as shown in Fig. 10). Generally speaking, we have found that agreement between phase diagrams calculated with and without concentration-dependent forms increases at the high-polymer end. And, except for the location, shapes of the binodal and spinodal curves are similar in both cases. Consequently, for modeling purposes, NS-S-P phase diagrams could be calculated without serious error, using reasonably constant g_{12} parameters characteristic of the experimental range.

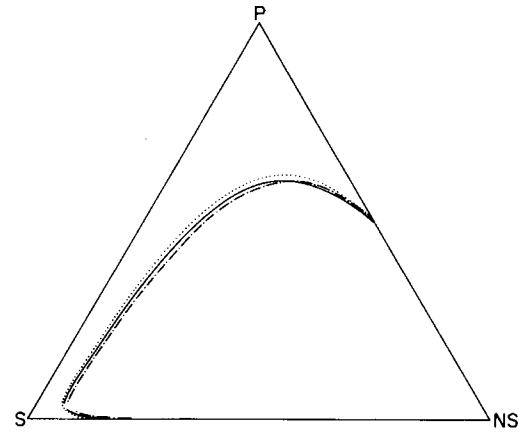

Fig. 9. Spinodal curves for (–) a concentration-dependent g_{12}, ($g_{12} = -0.218 - 0.861u_2 + 0.383u_2^2$) and for two constant g_{12} values: (–•–) $g_{12} = -0.55$; (• • •) $g_{12} = -0.7$. Other parameters are $\nu_1/\nu_2 = 0.2$, $\nu_1/\nu_3 = 0.002$, $g_{13} = 1.0$, and $g_{23} = 0.2$.

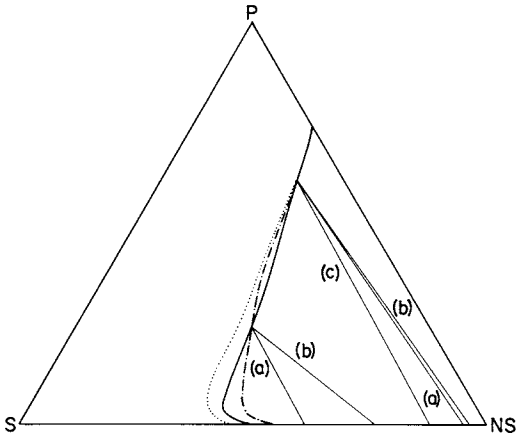

Fig. 10. Binodal curves for (–) a concentration-dependent g_{12} ($g_{12} = 1.141 - 0.457u_2 + 1.528u_2^2$) and associated tie lines (a), compared to constant $g_{12} = 1.1$ (–•–) with associated tie lines (b), and constant $g_{12} = 0.8$ (• • •) with associated tie lines (c). Other parameters are $\nu_1/\nu_2 = 0.25$, $\nu_{1,\nu 3} = 0.002$, $g_{13} = 1.1$, and $g_{23} = 0.4$.

Solvent–Polymer Interactions

Data for the concentration dependence of solvent–polymer interaction parameters are unfortunately quite limited. The tabulation by Orwoll[12] for a number of binary systems illustrates that relatively few values of g_{23} have been obtained over reasonable ranges of concentration. These are listed in Table IV. As mentioned before, in consequence of the limited number of points in each case (typically four to eight) and inherent experimental difficulties limiting their accuracy,[16] we chose to limit ourselves to empirical fits of low order for correlation. Likewise, the form mentioned earlier, suggested by Koningsveld and Kleintjens, was used.

$$g_{23} = \alpha + \frac{\beta}{1 - \gamma\phi_3} \tag{22}$$

where now α, β, and γ are constants for the solvent–polymer system. The range of parameters resulting from the fits of these forms to the data of Table IV is given in Table V.

A large number of phase-diagram calculations were carried out, from which we have been able to draw a number of important observations and conclusions regarding trends. From Table V, one sees that the interaction parameters do not in general exhibit uniform behavior with increasing polymer concentration, and, on the basis of the error criterion, preference for a particular form would not be obvious. On the other hand, for cases where the γ parameter in eq. (22) is equal to or greater than unity, a discontinuity in g_{23} can occur somewhere in the range $0 \leq \phi_3 \leq 1$. In addition, on the basis of the lattice model,[33] one would expect γ to fall between 0 and 1. Inspection of Table V shows that in five of nine cases, $\gamma > 1$, whereas for the remaining four, it is less than zero. Thus on purely

TABLE IV
Range and Behavior of Solvent–Polymer Interaction Parameters

System	Experiments range of polymer concentrations	Range of interaction parameters	Behavior with increasing concentration	Reference
1. CA–dioxane	0.1 –0.4	0.23–0.53	Monotonic increase	26
2. CA–methyl acetate	0.07–0.4	0.17–0.60	Monotonic increase	26
3. CA–pyridine	0.1 –0.37	0.05–0.22	Decrease at low concentration followed by very slow increase	26
4. CN–acetone	0.05–0.29	0.2 –(–0.93)	Very slow increase at low concentration, followed by rapid decrease	26
5. CN–methyl acetate	0.06–0.32	0.16–(–1.06)	Same as above	26
6. PVA–benzene	0.38–0.92	0.25–0.48	Monotonic decrease	27
7. PVA–vinyl acetate	0.38–0.86	0.21–0.51	Same as above	27
8. CA–acetone	0.1 –0.36	0.05–0.5	Monotonic increase	26
9. Polyisobutene-*n*-pentane	0.08–0.75	0.49–0.64	Increases until near the end of the concentration range, then decreases	28

TABLE V
Correlations for Concentration-dependent Solvent–Polymer Interaction Parameters

System[a]	Coefficients for $g_{23} = a + b\phi_3$		Sum of Squares	Coefficients for $g_{23} = a + b\phi_3 + C\phi i^2$			Sum of squares	Coefficients for $g_{23} = \alpha + \beta/(1 - \gamma\phi_3)$			Sum of squares
	a	b		a	b	c		α	β	γ	
1	.118	.984	1.29×10^{-4}	.099	1.151	−.309	6.73×10^{-5}	3.658	−3.559	−.327	6.98×10^{-5}
2	.147	1.206	1.46×10^{-2}	.0069	2.728	−3.2363	4.98×10^{-3}	.84	−1.026	−7.45	3.52×10^{-3}
3	.201	.469	1.04×10^{-2}	.48	−3.176	5.719	1.63×10^{-3}	.042	−.038	11.04	5.33×10^{-4}
4	.662	−4.294	3.47×10^{-1}	−.209	8.966	−39.91	2.33×10^{-2}	.513	−.198	3.05	1.99×10^{-2}
5	.616	−4.322	2.21×10^{-1}	−.119	5.445	−25.89	1.01×10^{-2}	.609	−.351	2.48	6.96×10^{-3}
6	.615	−.406	2.24×10^{-3}	.609	−.387	−.014	2.24×10^{-3}	.362	.0046	1.54	3.54×10^{-2}
7	.637	−.519	8.49×10^{-3}	.952	−1.631	.905	5.25×10^{-3}	−.859	1.682	−.732	1.17×10^{-2}
8	.025	1.338	9.72×10^{-4}	−.197	3.204	−3.582	2.65×10^{-5}	.928	−1.409	−6.252	7.4×10^{-5}
9	.487	.224	2.28×10^{-3}	.467	.356	−.163	1.77×10^{-3}	−.566	−.0049	2.142	1.48×10^{-2}

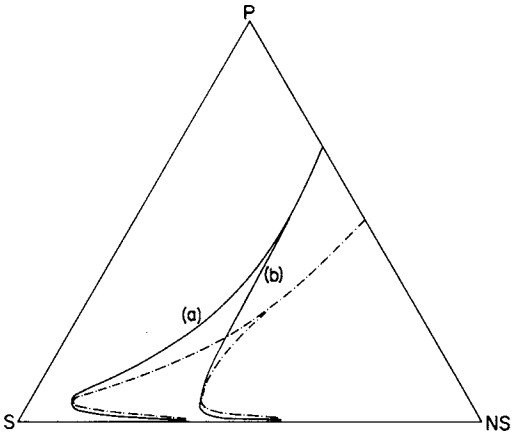

Fig. 11. Phase diagrams showing (–) binodal curves and (–•–) associated spinodal curves for concentration-dependent $g_{23} = 0.201 - 0.469\phi_3$ (curve a) and constant $g_{23} = 0.2$ (curve b). Other parameters are $\nu_1/\nu_2 = 0.25$, $\nu_1/\nu_3 = 0.002$, $g_{12} = 0.5$, and $g_{13} = 1.0$.

empirical grounds, on the basis of these data the assumed form appears inconsistent. As further illustrated in Table IV, with the exception of the polyisobutene-*n*-pentane system, the lmited concentration range over which data are available means that one is necessarily extrapolating the functional forms for g_{23} in the generation of the complete phase diagram. Because parabolic functions are generally inappropriate for extrapolation and too few data are available to justify third-order fits, we conclude that despite their relatively poor accuracy, linear functions are more appropriate for extrapolation.

Figures 11 and 12 illustrate typical effects on the phase diagram resulting from use of the concentration-dependent g_{23} as compared to constant values. In many cases we found that regardless of the g_{23} value chosen, it was not

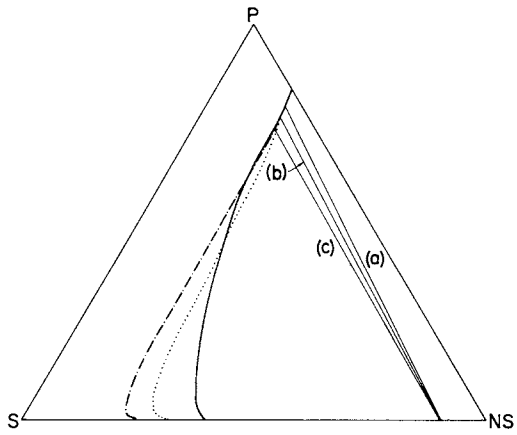

Fig. 12. Binodal curves for (–) concentration-dependent $g_{23} = 0.099 + 1.15\phi_3 - .309\phi_3^2$ with associated tie line (a); for (• • •) constant $g_{23} = 0.0$ with associated tie line (b); and for (–•–) constant $g_{23} = 0.4$ with associated tie line (c). Other parameters are $\nu_1/\nu_2 = 0.21$, $\nu_1/\nu_3 = 0.002$, $g_{12} = 0.8$, and $g_{13} = 1.4$.

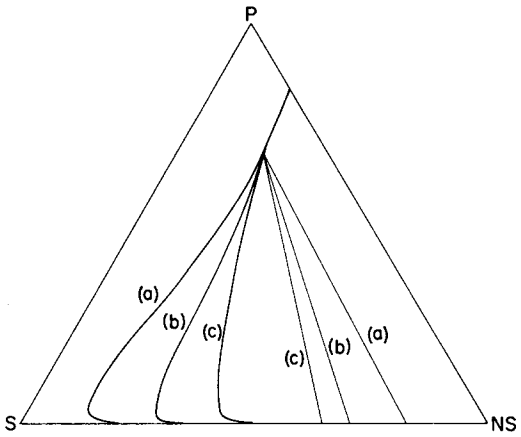

Fig. 13. Binodals and associated tie lines for various g_{23}: (a) $g_{23} = 0.5$, (b) $g_{23} = 0.1$, (c) $g_{23} = 0.025 + 1.338\phi_3$. Other parameters are $\nu_1/\nu_2 = 0.25$, $\nu_1/\nu_3 = 0.002$, $g_{12} = 0.8$, and $g_{13} = 1.4$.

possible to obtain good agreement. As shown in Figure 11, shape differences as well as magnitude changes can in some cases be quite severe. One also sees the general feature that differences are greatest in the moderately low polymer range. In some cases, a constant value outside the actual experimental range is needed, as is seen, for example, in Figure 12, where the constant value of 0.0 for g_{23} is smaller than any actually measured for that system.

Comparison of Figures 13 and 14 illustrates that shape changes are more pronounced for the spinodal curves. Consequently, the use of accurate concentration-dependent forms for the solvent–polymer system becomes critical if one requires a knowledge of the spinodal for the membrane-formation process calculation.[4,10]

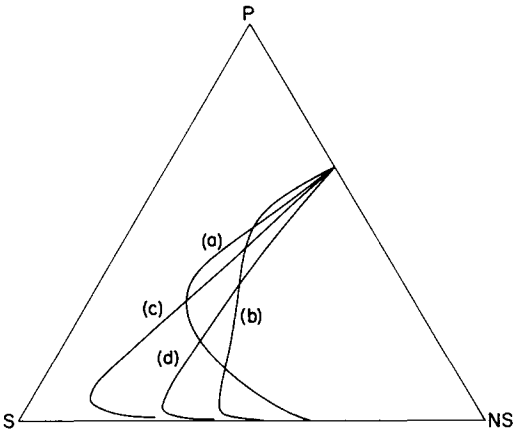

Fig. 14. Spinodal curves for various g_{23}: (a) $g_{23} = 0.928 - [1.409/(1 + 6.252\phi_3)]$, (b) $g_{23} = 0.025 + 1.338\phi_3$, (c) $g_{23} = 0.5$, (d) $g_{23} = 0.0$. Other parameters are $\nu_1/\nu_2 = 0.25$, $\nu_1/\nu_3 = 0.002$, $g_{12} = 0.8$, $g_{13} = 1.4$.

CONCLUSIONS

These results show the critical role of the concentration dependence of the solvent–polymer interaction parameter in affecting the nature of the predicted miscibility gap. These calculations further indicate that, until data covering wider concentration ranges are available, the use of a linear form for g_{23} is considered the most defensible. Contrary to the conclusion of a previous study,[9] we have shown that the concentration dependency of the solvent–polymer interaction parameter is more important in the control of the phase diagram behavior than that of the nonsolvent–solvent parameter.

References

1. S. Loeb and S. Sourirajan, *Adv. Chem. Ser.*, **38**, 117 (1963).
2. R. E. Kesting, *Synthetic Polymer Membranes*, McGraw-Hill, New York, 1971.
3. M. N. Sarbolouki, *J. Polym. Sci., Polym. Lett. Ed.*, **11**, 753 (1973).
4. L. Yilmaz, Ph.D. thesis, University of Illinois, Urbana, 1986.
5. R. L. Scott, *J. Chem. Phys.*, **17**, 268 (1949).
6. W. R. Krigbaum and D. K. Carpenter, *J. Polym. Sci.*, **14**, 241 (1954).
7. K. W. Suh and D. W. Liou, *J. Polym, Sci., A-2*, **6**, 813 (1968).
8. H. Tompa, *Polymer Solutions*, Butterworths London, 1956.
9. F. W. Altena and C. A. Smolders, *Macromolecules*, **15**, 1491 (1982).
10. C. Cohen, G. B. Tanny, and S. Prager, *J. Polym. Sci., Polym. Phys. Ed.*, **17**, 477 (1979).
11. D. M. Koenhen, M. H. V. Mulder, and C. A. Smolders, *J. Appl. Polym. Sci.*, **21**, 199 (1977).
12. R. A. Orwoll, *Rubber Chem. Technol.*, **50**, 451 (1977).
13. W. R. Moore and R. Shuttleworth, *J. Polym. Sci.*, **A1**, 733 (1963).
14. A. Nakajima, H. Yamakawa, and I. Sakurada, *J. Polym. Sci.*, **35**, 489 (1959).
15. L. H. Baker, W. B. Brown, G. Gee, J. S. Rowlinson, D. Stubley, and R. E. Yeadon, *Polymer*, **3**, 215 (1962).
16. R. Corneliussen, S. A. Rice, and H. Yamakawa, *J. Chem. Phys.*, **38**, 1768, (1963).
17. P. J. Flory, *Principles of Polymer Chemistry*, Cornell University Press, Ithaca, NY, 1953.
18. J. W. Kennedy, *Macromol. Chem. (London)*, **1**, 296 (1980).
19. P. W. Thornley and I. W. Shepherd, *J. Polym. Sci., Polym. Phys. Ed.*, **15**, 1339 (1977).
20. A. Horta, *Macromolecules*, **12**, 785 (1979).
21. J. Pouchly, A. Zivney, and K. Solc, *J. Polym. Sci., Polym. Symp.*, **23**, 245 (1968).
22. S. G. Chu and P. Munk, *Macromolecules*, **11**, 879 (1978).
23. C. C. Hsu and J. M. Prausnitz, *Macromolecules*, **7**, 320 (1974).
24. C. G. Guffey and A. H. Wehe, *A.I.Ch.E. J.*, **18**, 914 (1972).
25. M. Guillotin, C. Lemoyne, C. Noel, and L. Monnerie, *Desalination*, **21**, 165 (1977).
26. C. Lemoyne, J. L. Halary, C. Friedrich, C. Noel, and L. Monnerie, *J. Appl. Polym. Sci.*, **25**, 1883 (1980).
27. L. Broens, F. W. Altena, C. A. Smolders, and D. M. Koenhen, *Desalination*, **32**, 33 (1980).
28. M. H. V. Mulder and C. A. Smolders, *J. Memb. Sci.*, **27**, 289 (1984).
29. A. Dondos, P. Rempp, and H. Benoit, *J. Polym. Sci., Part C*, **30**, 9 (1970).
30. E. F. Casassa, *J. Polym Sci., Part C*, **54**, 53 (1976).
31. J. Pouchly and A. Zivny, A. *Makromol. Chem.*, **183**, 3019 (1982).
32. R. V. Orye and J. M. Prausnitz, *Ind. Eng. Chem.*, **57**, 18 (1965).
33. R. Koningsveld and L. A. Kleintjens, *Macromolecules*, **4**, 637 (1971).

Received April 11, 1985
Accepted June 10, 1985